Impact of hydraulic retention time on community assembly and function of photogranules for wastewater treatment

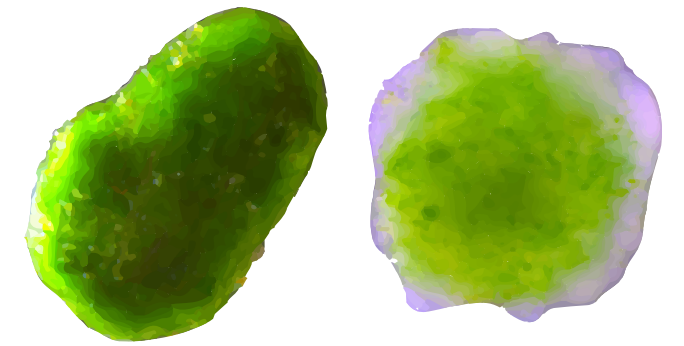Trebuch, L. M., Oyserman, B. O., Janssen, M., Wijffels, R. H., Vet, L. E. M., & Fernandes, T. V.
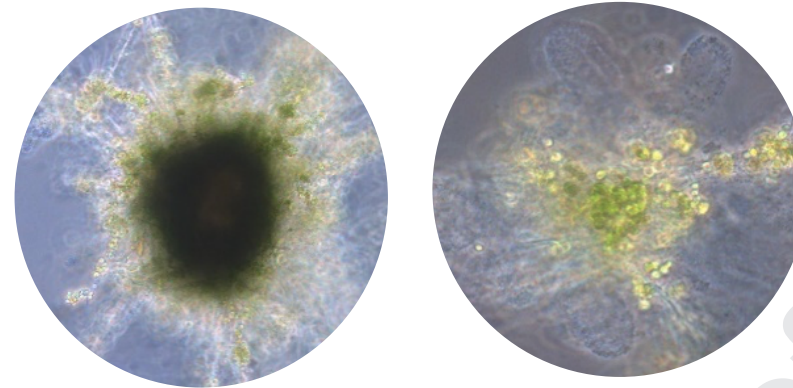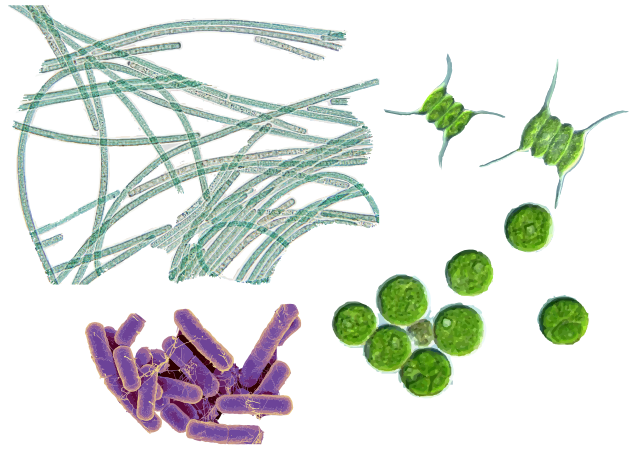
Community assembly and structure of photogranules

Free suspended cells → Floccular aggregation → Photogranulation

Cyanobacteria

Microalgae

Nitrifiers

PAOs

Denitrifiers

Biofilm formers

1 **Impact of hydraulic retention time on community assembly and function of**

2 **photogranules for wastewater treatment**

3 Lukas M. Trebuch* [1,4], Ben O. Oyserman[2,3], Marcel Janssen [4], René H. Wijffels [4,6], Louise E. M. Vet [5], Tânia V.

4 Fernandes [1]

5 [1] *Department of Aquatic Ecology, Netherlands Institute of Ecology (NIOO-KNAW), Droevendaalsesteeg 10,*

6 *6708 PB Wageningen, The Netherlands*

7 [2] *Department of Microbial Ecology, Netherlands Institute of Ecology (NIOO-KNAW), Droevendaalsesteeg 10,*

8 *6708 PB Wageningen, The Netherlands*

9 [3] *Bioinformatics Group, Wageningen University, Wageningen, The Netherlands*

10 [4] *Bioprocess Engineering, AlgaePARC Wageningen University, P.O. Box 16, 6700 AA Wageningen, The*

11 *Netherlands*

12 [5] *Department of Terrestrial Ecology, Netherlands Institute of Ecology (NIOO-KNAW), Droevendaalsesteeg 10,*

13 *6708 PB Wageningen, The Netherlands*

14 [6] *Faculty of Biosciences and Aquaculture, Nord University, N-8049, Bodø, Norway*

15 *-Corresponding author: L.Trebuch@nioo.knaw.nl, +4369918110088

16 **1. Abstract**

17 Photogranules are dense, spherical agglomerates of cyanobacteria, microalgae and non-phototrophic

18 microorganisms that have considerable advantages in terms of harvesting and nutrient removal rates

19 for light driven wastewater treatment processes. This ecosystem is poorly understood in terms of the

20 microbial community structure and the response of the community to changing abiotic conditions. To

21 get a better understanding, we investigated the effect of hydraulic retention time (HRT) on

22 photogranule formation and community assembly over a period of 148 days. Three laboratory

23 bioreactors were inoculated with field samples from various locations in the Netherlands and operated

24 in sequencing batch mode. The bioreactors were operated at four different HRTs (2.00, 1.00, 0.67,

25 0.33 days), while retaining the same solid retention time of 7 days. A microbial community with

26 excellent settling characteristics (95-99% separation efficiency) was established within 2 to 5 weeks.

27 The observed nutrient uptake rates ranged from 24 to 90 mgN L^{-1} day^{-1} and from 3.1 to 5.4 mgP L^{-1}

28 day^{-1} depending on the applied HRT. The transition from single-cell suspension culture to floccular

29 agglomeration to granular sludge was monitored by microscopy and 16S/18S sequencing. In

30 particular, two important variables for driving aggregation and granulation, and for the structural

31 integrity of photogranules were identified: 1. Extracellular polymeric substances (EPS) with high

32 protein to polysaccharide ratio and 2. specific microorganisms. The key players were found to be the

33 cyanobacteria *Limnothrix* and *Cephalothrix*, the colony forming photosynthetic eukaryotes within

34 *Chlamydomonadaceae*, and the biofilm producing bacteria *Zoogloea* and *Thauera*. Knowing the

35 makeup of the microbial community and the operational conditions influencing granulation and

36 bioreactor function is crucial for successful operation of photogranular systems.

37 **Keywords:** *Microalgae and cyanobacteria; phototrophic granulation; extracellular polymeric*

38 *substances; metagenomics; microbial ecology; functional network*

2. Introduction

40 Biological wastewater treatment systems are ubiquitous and essential for maintaining high water

41 quality and prevent excess discharge of nutrients and pollutants into the environment (Henze, 2008).

42 However, wastewater treatment also comes at a cost as it is an energy intensive process (McCarty et

43 al., 2011) and contributes to greenhouse gas emissions (Cakir and Stenstrom, 2005). Hence, improving

44 the efficacy and sustainability of these systems through technological innovation may have broad scale

45 impacts on global sustainability. The incorporation of phototrophic organisms, such as microalgae and

46 cyanobacteria, shows great potential in improving the sustainability of treatment processes by

47 mitigating greenhouse gasses (Smith et al., 2010), closing nutrient cycles (Fernandes et al., 2015),

48 matching wastewater N:P ratio for effective treatment by using phototrophic consortia (Fernandes et

49 al., 2017), and providing oxygen to drive processes such as nitrification and polyphosphate

50 accumulation (Oyserman et al., 2017). While promising, one of the current bottlenecks in the wider

51 application of phototrophic communities in wastewater treatment is the harvesting of the biomass.

52 A principal operational parameter which ensures the effectiveness and economic feasibility of

53 treatment is to retain the microbial community as dense biomass within the treatment system (Ardern

54 and Lockett, 1914; Milferstedt et al., 2017a). This requires operational parameters which steer the

55 microbial community to form natural and well settling aggregates. These aggregates may be described

56 as either flocs or granules, depending on their structure, density, and settleability. In general, granules

57 are discrete well-defined microbial aggregates formed by cell-to-cell attraction with regular dense and

58 strong structure, and excellent settleability. Although the first granules were discovered over 50 years

59 ago (Lettinga et al., 1980), the biological mechanisms driving granule formation and the operational

60 parameters that select for their formation are still relatively unknown (Wilén et al., 2018). This

61 complex microbial function is far from being fully understood and bears many ecological questions

62 that need to be answered.

63 Merging granule technology with other biochemical processes such as photosynthesis holds the

64 promise of producing well settling photoautotrophic systems in so called photogranules. In general,

65 photogranules can be described as spherical biofilm systems of phototrophic and heterotrophic

66 microorganism. Photogranules were already obtained from different seeding cultures: (1)

67 hydrostatically incubated activated sludge (Abouhend et al., 2018), (2) activated granular sludge

68 mixed with unicellular green algae (Liu et al., 2017), and have demonstrated to work at lab-scale in

69 airlift reactors as well as in aeration-free mechanically stirred reactors (Meng et al., 2019; Tiron et al.,

70 2017). Photogranules are commonly cultivated in sequencing batch operation to provide cyclic wash-

71 out conditions, assure selection of well-settling biomass and prevent growth of individual cells in

72 suspension. This operation strategy is similar to the one applied in aerobic granular sludge technology

73 and assures a selection pressure for granular morphology (de Kreuk, 2006).

74 Motile filamentous cyanobacteria showed to be an important constituent of photogranule formation

75 and vital under static incubation and mixed operation conditions (Abouhend et al., 2018; Milferstedt et

76 al., 2017b). In green algae dominated photogranules, *Zoogloea* was shown to be involved in the

77 granulation process due to EPS production (Huang et al., 2015; Zhang et al., 2018). Few studies also

78 addressed other functional groups such as nitrifiers (Abouhend et al., 2018; Huang et al., 2015; Tiron

79 et al., 2015), denitrifiers (Stauch-White et al., 2017) or polyphosphate accumulating organisms

80 (PAOs) (Cai et al., 2019) in photogranules. However, successful implementation of photogranular

81 technology will require a deeper biological understanding of the processes and the microbial

82 community that drive granular structure and function so that this knowledge may be parameterized

83 both under static and hydrodynamic conditions. Integrating systems biology and community-based

84 approaches can provide significant insight into the physiology and role of specific organisms in

85 community function (Oyserman et al., 2016) which can help identify additional operational strategies

86 to steer biomass characteristics towards a particular ecosystem function. Therefore, in order to fully

87 exploit photogranule technology, a first step is linking information about the microbial ecology of

88 phototrophic granulation with properties of the granules.

89 In this study we examined the effect of hydraulic retention time (HRT) on the function and assembly

90 of a photogranular community. By using amplicon sequencing, microscopic observation,

91 characterization of the EPS matrix and general acquisition of reactor performance, key organisms and

92 factors can be identified. We compared taxonomical & functional groups correlation with chemical

4

93   and physical data from the bioreactor system to identify potential biological drivers of key functional

94   properties. This will enhance the understanding of photogranular systems and help to further improve

95   the operational strategies.

Materials and Methods

2.1. Algal-bacterial community

The reactors were inoculated with biomass from nutrient rich sources at equal proportions by mass. The inoculum comprised out of field samples from various locations in the Netherlands and sludge from an upflow anaerobic sludge blanket (UASB) reactor operated 35°C and 8 days HRT at the Netherlands Institute of Ecology (NIOO-KNAW), The Netherlands. The field samples were taken in selected places with high temperature and nutrient loading. They originate from a tropical (35°C) fish breeding aquarium, a eutrophic small pond at a farm and a clarifier of the wastewater treatment plant of the paper industry PARENCO B.V. (Renkum, The Netherlands). In addition, two microalgal laboratory strains used in previous research on wastewater at NIOO-KNAW (Fernandes et al., 2015), *Chlorella sorokiniana* and *Chlorococcum* sp. from the culture collection at NIOO-KNAW were added. The final mixture of algae and bacteria was inoculated with equal proportions in terms of biomass concentration with a final density of 0.025 g L^{-1}. After 10 days of cultivation in batch biomass reached a concentration of approximately 2 g L^{-1}.

2.2. Experimental set-up

Three 1.7 L bubble column bioreactors were operated for 116 days as sequencing batch reactors with HRTs of 2.00, 1.00 and 0.67 days. From day 116 to the end of the experiment (day 148), the 2.00 d HRT bioreactor was changed to 0.67 d and the 1.00 d HRT bioreactor was changed to 0.33 d. The third bioreactor was kept at the same condition (HRT of 0.67 d). The operation procedure of each 12h (2.00, 1.00, 0.67 d HRT) or 6h (0.33 d HRT) cycle was: 30 min of settling, 15 min of decanting, 15 min of filling and 660 min (12h cycle) and 300 min (6h cycle) reaction time. After decanting, synthetic wastewater (modified BG-11 medium) was added with following composition: 472.0 mg L^{-1} $(NH_4)_2SO_4$, 56.0 mg L^{-1} K_2HPO_4, 75.0 mg L^{-1} $MgSO_4.7H_2O$, 420 mg L^{-1} sodium acetate trihydrate, 36.0 mg L^{-1} $CaCl_2.2H_2O$, 8.4 mg L^{-1} EDTA ferric sodium salt, 1.8 mg L^{-1} $Na_2EDTA.2H_2O$, 2.86 mg L^{-1} H_3BO_3, 1.81 mg L^{-1} $MnCl_2.4H_2O$, 0.44 mg L^{-1} $ZnSO_4.7H_2O$, 0.079 mg L^{-1} $CuSO_4.5H_2O$, 0.22 mg L^{-1} $Na_2MoO_4.2H_2O$, 0.05 mg L^{-1} $Co(NO_3)_2$ $6H_2O$, 0.12 mg L^{-1} Vitamin B_1 and 0.0012 mg L^{-1} Vitamin B_{12}.

6

122   The final concentrations of the major constituents are: 100 mg_N L^{-1}, 10 mg_P L^{-1}, 200 mg_{COD} L^{-1}. The

123   nutrient load per day for each HRT are summarized in **Table A1** in the supplemental material. For

124   each reactor, a solid retention time of 7 days was achieved by decanting the settled biomass twice a

125   week to lower the biomass concentration to 1 g L^{-1}. The biomass concentration within the bioreactor

126   before harvesting the biomass was usually between 2-3 g L^{-1}.

127   Each glass bioreactor had an inner diameter of 0.10 m and a conical bottom part and was illuminated

128   from one side with two warm-white LED flood lights providing an incident light intensity of 500 μmol

129   m^{-2} s^{-1} (PAR range) at the reactor surface. Illumination followed a 12:12 (light:dark) cycle which

130   resulted in an total light input of 0.68 mol_{ph} $reactor^{-1}$ day^{-1}, or 0.4 mol_{ph} L^{-1} day^{-1}, considering the

131   reactor geometry. The bioreactors were aerated with 400 $mL.min^{-1}$ of 5% CO_2 enriched air (regulated

132   by mass flow controllers) to ensure non-limiting inorganic carbon conditions and mixing of the

133   culture. Temperature was controlled at 35 °C by water baths and pH was controlled at 6.7±0.1 by

134   automatic addition of 1M HCl and 1M NaOH by pH controllers.

2.3. Analytical Methods

136   Daily samples for NH_4^+–N, PO_4^{3-}–P, NO_3^-–N, and NO_2^--N analysis were filtered through a 0.2 μm

137   cellulose acetate filter (VWR) and measured in a Seal QuAAtro39 AutoAnalyzer (SEAL Analytical

138   Ltd., Southampton, UK) according to standard protocols (APHA/AWWA/WEF, 2012). Total

139   inorganic nitrogen is the sum of NH_4^+–N, NO_3^-–N, and NO_2^--N measured in liquid. Biomass dry

140   weight (DW), elemental composition and sludge volume index (SVI) of the algal-bacterial biomass

141   was determined according to standard methods (APHA/AWWA/WEF, 2012). The separation

142   efficiency (SE) of the biomass was calculated from the biomass concentration of the total reactor

143   content and effluent (equation A1 in supplemental information). The elemental composition of

144   homogenized freeze-dried biomass was measured. For C and N analyses a subsample (about 2mg) was

145   folded into a tin cup and analysed with an organic elemental analyzer (Flash 2000, Interscience

146   Breda). Cellular P was analysed by combusting a subsample (about 2mg) for 30min at 550°C in Pyrex

147   glass tubes, followed by a digestion step with 10 mL persulfate (2.5%) for 30 min at 121°C. The

148   digested solution was measured for PO_4^{3-} on a Seal QuAAtro39 AutoAnalyzer (SEAL Analytical Ltd.,

149 Southampton, UK). Extracellular polymeric substances (EPS) were extracted with the formamide-

150 sodium hydroxide method according to Adav and Lee (2008). Total polysaccharides were measured

151 with the phenol-sulfuric method (DuBois et al., 1956), and total proteins with the modified Lowry

152 method using Modified Lowry Protein Assay Kit (ThermoFisher Scientific, USA) (Lowry et al.,

153 1951). The results are given in polysaccharide and protein content of EPS, which are abbreviated with

154 EPS-PS and EPS-PN. Both, EPS extractions and measurements of total polysaccharides and proteins

155 were performed in triplicates. Microscopic observations were performed with a fluorescence

156 microscope (Leica DMI4000 B, Germany) and a stereo microscope (Leica M2015C). Pictures were

157 obtained with the software Cell* (Soft Imaging Systems GmbH, Germany) and Leica Application

158 Suite (LAS version 4.7).

159 **2.4. Statistical analysis**

160 The acquired physical, chemical and biological data of all applied HRTs were summarized and quasi-

161 steady state conditions were statistically compared by one factor ANOVA with Tukey's HSD as a post

162 hoc test (**table A2**). In the case of HRT 0.67d, the dataset of two bioreactors (R1 & R3) operated at the

163 same HRT were combined to one.

164 **2.5. Metagenomics/High-throughput sequencing**

165 From each reactor, biomass was sampled at nine time points. The initial inoculum, after 10 days batch

166 phase and start of experiment (referred to as day 0), and days 11, 25, 32, 60, 82, 119 and 140

167 respectively. DNA extraction from each time point was conducted in triplicate. In addition, the starting

168 inoculum was also extracted in triplicate. Specifically, 15 mL of harvested sludge was centrifuged at

169 5500 rpm and the supernatant discarded. The cell pellets were immediately frozen at -80 °C until

170 further processing. DNA was extracted by using the DNeasy PowerSoil Isolation Kit (Qiagen GmbH,

171 Hilden, Germany). The quantity and quality of DNA were spectrophotometrically determined with a

172 NanoDrop (ThermoFisher Scientific, USA). The 75 genomic DNA samples were submitted for

173 sequencing to Génome Québec (MacGill University, Montreal, CA). The 16S rRNA gene V3/V4

174 variable region was amplified using primer pair 341F (CCTACGGGNGGCWGCAG) and 805R

8

175   (GACTACHVGGGTATCTAATCC) (Herlemann et al., 2011). The 18S rRNA gene V4 variable

176   region was amplified using the primer pair 616*F (TTAAARVGYTCGTAGTYG) and 1132R

177   (CCGTCAATTHCTTYAART) (Hugerth et al., 2014). Both sets of primers were modified to add

178   Illumina adapter overhang nucleotides sequences to the gene-specific sequences. Sequencing was

179   performed using an Illumina MiSeq system (Illumina MiSeq, USA) with 300-bp reads (v3 chemistry).

180   The obtained sequences were processed with the Hydra pipeline version 1.3.3 (Hollander, 2018)

181   implemented in Snakemake (Köster and Rahmann, 2012). Taxonomic alignment of the sequences was

182   done to the SILVA database (release 132) using SINA (https://www.arb-silva.de). The analysis of the

183   microbiome data was performed with the R-package phyloseq (version 1.26.1) (McMurdie and

184   Holmes, 2013). All high-throughput sequencing data are deposited in the National Center for

185   Biotechnology Information database and can be found under the accession number SAMN12373400-

186   SAMN12373549 and under the SRA bioproject PRJNA556418.

187   **2.6. Raw read processing**

188   A total of 7.869.303 16S and 8.723.187 18S raw reads were generated. After quality trimming, adapter

189   trimming and length filtering using cutadapt version 1.18 (Martin, 2013), the Hydra pipeline version

190   1.3.3 (Hollander, 2018) implemented in Snakemake (Köster and Rahmann, 2012) was used to merge

191   paired end reads and cluster OTUs. A total of 3.748.927 16S and 2.306.332 18S contigs remained that

192   were further processed using the R package phyloseq version 1.26.1 (McMurdie and Holmes, 2013).

193   In the downstream process the 16S and 18S data set was normalized using the cumulative sums

194   scaling (CSS) function of the R package metagenomSeq version 1.24.1 (Paulson et al., 2013). The

195   community structure and the change through time of the 16S and 18S dataset were analysed by

196   Principal Coordinate Analysis (PCoA) of a Bray-Curtis dissimilarity matrix. For clustering the 16S

197   and 18S dataset were subsetted to the top 20 OTUs and known functional groups based on the MIDAS

198   database (McIlroy et al., 2015) and Milferstedt et al. (2017b) (table A4 in supplemental information)

199   **2.7. Correlation network analysis**

200 Pearson correlation coefficient (PCC) between microbial data and functional parameter (table A5 in

201 supplemental materials) obtained from the reactor operations were determined with the R function *cor*

202 in the R package *stats* version 3.5.2. A threshold of > 0.5 and <-0.5 for the PCC was used to filter

203 OTUs only correlating strongly with functional parameters. This threshold was greater than 2 standard

204 deviations from the mean PCC. The software Cytoscape 3 was used to analyse the correlation network

205 and to visually represent the network (Su et al., 2014).

3. Results

3.1. Photogranule formation

The development of a well settling algal-bacterial community was strongly influenced by the applied HRT. With decreasing HRT, and therefore increasing hydraulic pressure, the microbial community was driven more rapidly towards floccular aggregates. Specifically, at an HRT 0.67 d the assembly time was reduced to 11 days compared to 32 days at HRT 2.00. The hydraulic pressure dictated the SE as well, which resulted in better separation at lower HRTs. When changing the HRT at day 116 from 2.00 d to 0.67 d and from 1.00 d to 0.33 d the settling properties increased significantly and the microbial community shifted to be dominated by photogranules.

In **Figure 1,** the separation efficiency (SE) of biomass from the liquid is displayed as a percentage (%) of the total amount of biomass in the system. As HRT decreased, the separation efficiency of the biomass increased. Specifically, a SE higher than 90% in phase 1 was achieved for the reactor with an HRT of 0.67 d in 10 days. The reactor with an HRT of 1.00 d achieved this SE in 24 days of operation, whereas the reactor operated at an HRT of 2.00 d required 32 days. These results show that a lower HRT accelerated the assembly of flocs and granules by rapid selecting for well-settling biomass. The higher hydraulic pressure experienced by the microbial community at HRT 1.00 d, and below, drives a SE greater than 90%. Furthermore, in the case of HRT 0.67 d and HRT 0.33 d in phase 2 the SE increased to 99%. In **Figure 2A** the long-term effect of HRT on SE and SVI is depicted. A lower HRT drives a higher SE and lower SVI. The variability in SE and SVI was also lower with lower HRT, suggesting that low HRT increased the functional stability**.** This implies that it promotes a more stable settling and therefore improves biomass retention in the system. The increased SE was accompanied by a decrease in SVI. While the microalgal-bacterial community exhibited an SVI of >300 mL g^{-1} at the start of operation it was reduced to an average of 57 ± 9 mL.g^{-1} when it began to show granular biomass structure.
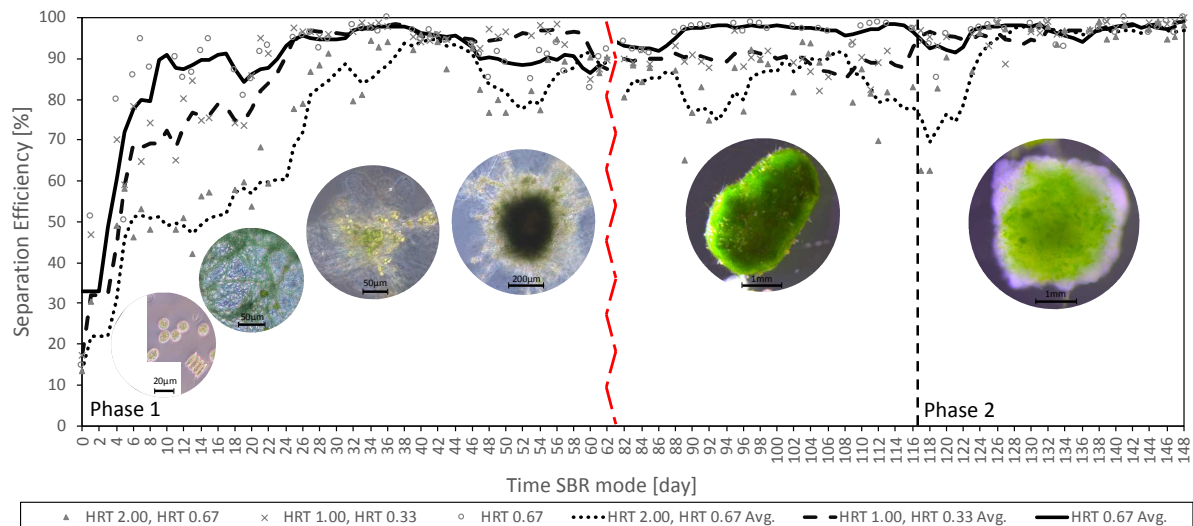
Figure 1. SE (%) of biomass of the 3 bioreactors over the course of the experiment. The first month is characterized by the assembly of the microbial community to well-settling biomass, while the following two months feature first photogranule appearance and further maturation. At day 116 (phase 2) a shift in the HRT was performed. The red dashed line at day 62 symbolizes a two-week period of not stringent monitoring. The microscopic images provided along the timeline are taken at following timepoints (from left to right): first 2 of eukaryotic green algae and motile filamentous cyanobacteria from the inoculum; next 2 at t=32 and t=60 of floccular aggregates; last 2 at t=82 and t=140 of photogranules. A scale bar is included in each picture.

The morphological changes of the photogranules during the operation were followed by microscopic observation with selected pictures shown in **Figure 1**. The inoculum consisted of free organisms such as green algae, cyanobacteria and bacteria. Motile filamentous cyanobacteria present in the inoculum started to entangle and form early aggregates as flocs in the first weeks of operation and started to incorporate other prokaryotes and colony-forming photosynthetic eukaryotes. After about 3 month of operation the first granular structures appeared as shown by the microscopic images of t=82 and 140 days in **Figure 1**.

It has been shown that EPS may act like a glue that promotes the spatial alignment of both algae and bacteria to agglomerates (Flemming et al., 2007). Characterisation of the EPS matrix in terms of proteins (EPS-PN) and polysaccharides (EPS-PS) showed that EPS is a substantial part of the floccular and granular biomass ranging from 8-34% (**Figure A4**). In **Figure 2B** the average EPS is depicted for the applied HRT. There is no significant difference in constituent (EPS-PN and EPS-PS), however there is a significant increase in PN/PS ratio with lower HRT. While being a substantial part from the first appearance of floccular structure there was a change from mostly EPS-PS to a majority of EPS-PN content. This is reflected in a shift from the PN/PS ratio in EPS from 1.0 to 6.6 at HRT 0.67. The

253 makeup of EPS in the photogranules in the last month of operation at HRT 0.67 was found to be

254 239 ± 42 mg_{EPS} g_{VSS}^{-1} with a PN/PS ratio of about 6.6.
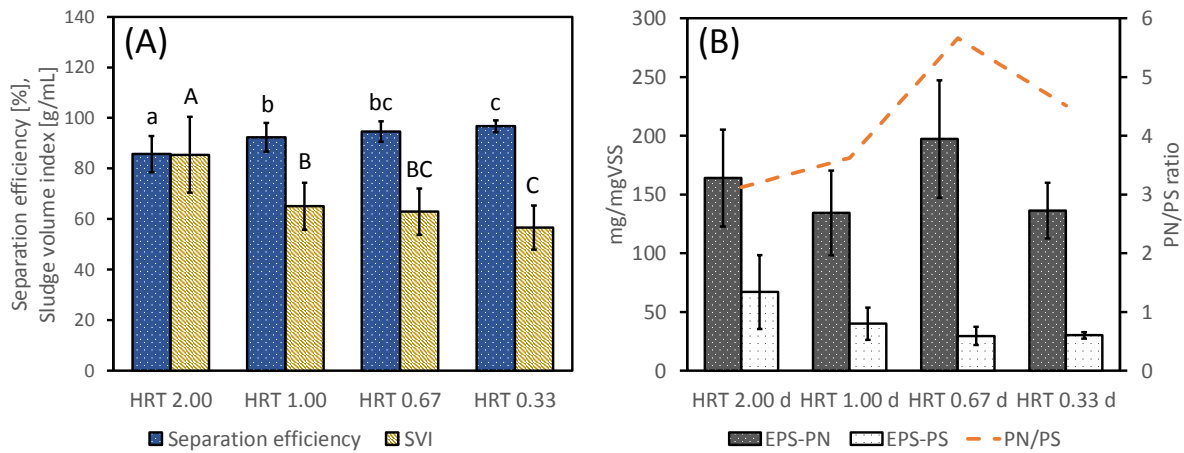

255

256 *Figure 2. (A) Relation between HRT, separation efficiency (SE) and sludge volume index (SVI) over applied HRT. The*
257 *standard deviation of the measured values is displayed as error bars. The letters (a, b, c, d, A, B, C, D) above the bars*
258 *indicate the significant difference between observations. (B) The EPS composition in terms of EPS-PN, EPS-PS and PN/PS*
259 *ratio (orange line) for each applied HRT.*

260 **3.2. Nutrient removal performance**

261 The initial phase of reactor operation was characterized by a rapid assembly of a well-settling floccular

262 microbial community with stable nitrogen and phosphorus removal after 2-4 weeks. In **Figure 3A** the

263 average volumetric nutrient removal rates across the applied HRT are shown. With decreasing HRT,

264 the volumetric removal rate for nitrogen increased significantly from 24 to 90 mg_N L^{-1} day^{-1} with the

265 maximum at HRT 0.33. After 40 days of operation nitrification started to occur in all three reactors,

266 but no stable nitrification rate was obtained until the end of operation (**Figure A1**). Since the increase

267 in nitrogen removal could not be explained with nitrogen assimilation in the biomass, the potential

268 denitrification was assessed. Therefore, a mass balance over nitrogen using in and out coming nitrogen

269 of the bioreactor, the biomass productivity and the elemental composition of the biomass was

270 performed. In that way it was shown that for HRT 0.67 denitrification accounted for 23% of the

271 nitrogen removal and for HRT 0.33 for 26% (**Figure A7**). The volumetric removal rate of phosphorus

272 increased with decreasing HRT from 3.1 to 5.4 mg_P L^{-1} day^{-1}, however not significantly. COD in the

273 form of acetate was fully consumed in all applied HRTs, which translates in a volumetric removal rate

274 of 97 to 580 mg_{COD} L^{-1} day^{-1} (**Figure A2**). With decreasing HRT, the biomass productivity increased

13

275 as well (**Figure 3B**). While there is no significantly difference in biomass productivity between HRT

276 2.00, 1.00 and 0.67, there was a significant increase at HRT 0.33. This can be explained due to the

277 increased COD load per day and the larger contribution of heterotrophic growth in the bioreactor
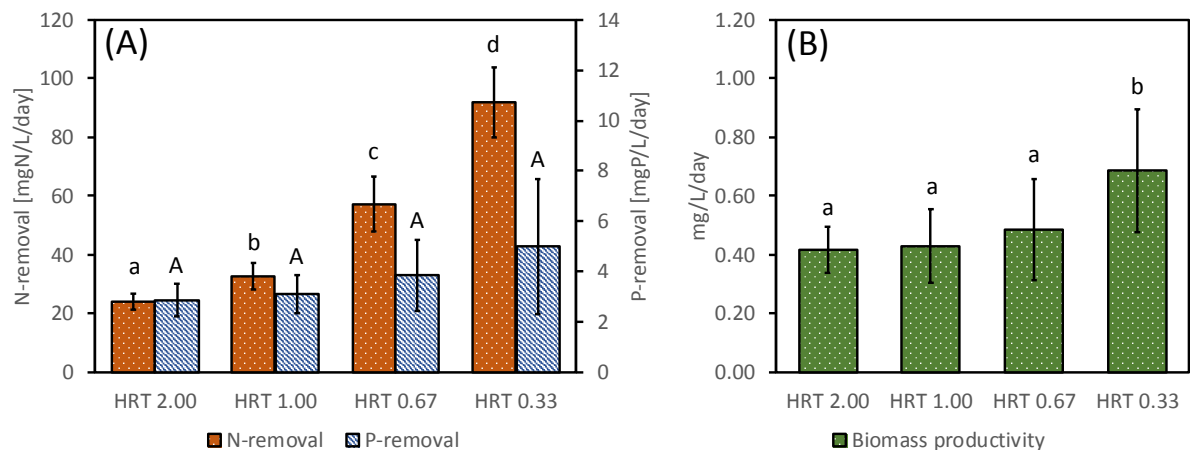
278 (**Figure A5**).

279

280 *Figure 3. (A): Volumetric nutrient removal rates per mol of photons of each applied HRT. All values shown are averaged*
281 *over the quasi-steady state conditions measurements. (B) Biomass productivity at the different HRTs applied. The error bars*
282 *are the standard deviation in the observed time frame. The letters (a, b, c, d, A) above the bars indicate the significant*
283 *difference between observations.*

284 In phototrophic systems the removal rates per mol of photon supplied are important to know next to

285 the volumetric removal rates. Considering a volumetric photon supply of 0.4 mol_{ph} L^{-1} day^{-1} the

286 removal rate per mol of photons range from 59 to 226 mg_N mol_{ph} day^{-1} nitrogen and 7.1 to 12.2 mg_P

287 mol_{ph} day^{-1} for phosphorus depending on the applied HRT. The biomass yield is ranging from 1.0-1.7

288 g_X mol_{ph} day^{-1}, which is higher than observed values for phototrophic growth due to the heterotrophic

289 growth that gets an increased importance at lower HRT.

290 **3.3. 16S and 18S rRNA-Gene-Based Microbial Community Assembly**

291 The principal coordinates analysis (PCoA) demonstrated tight clustering of triplicate samples for both

292 the 16S and 18S data sets (**Figure 4**). Thus, all downstream analysis on relative abundance for each

293 date was conducted using the average OTU read abundance from triplicates. The PCoA revealed a

294 clear and recurring trajectory of the prokaryotic and eukaryotic community from planktonic organisms

295 to the assembly of photogranules. Reactor 1 and 2 followed a similar trajectory, however, reactor 3,

296 which was operated at the lowest initial HRT of 0.67 days, diverged from the other two reactors at day

297   32, but then re-converged reaching the same general community structure by day 140. Interestingly, all

298   three reactors showed a similar 16S microbial community at day 140 regardless of the history of the

299   community and applied HRT. The 18S community showed more dynamic and did not reach a stable

300   community as the 16S one. In both PCoA plots a "horseshoe effect" is visible. This phenomenon is

301   often observed in microbiome studies that sample along an environmental gradients in which multiple

302   different niches are present and differentially represented (Morton et al., 2017). Here we show that this

303   horseshoe effect was also observed through time as microbiomes adapt to novel conditions from their
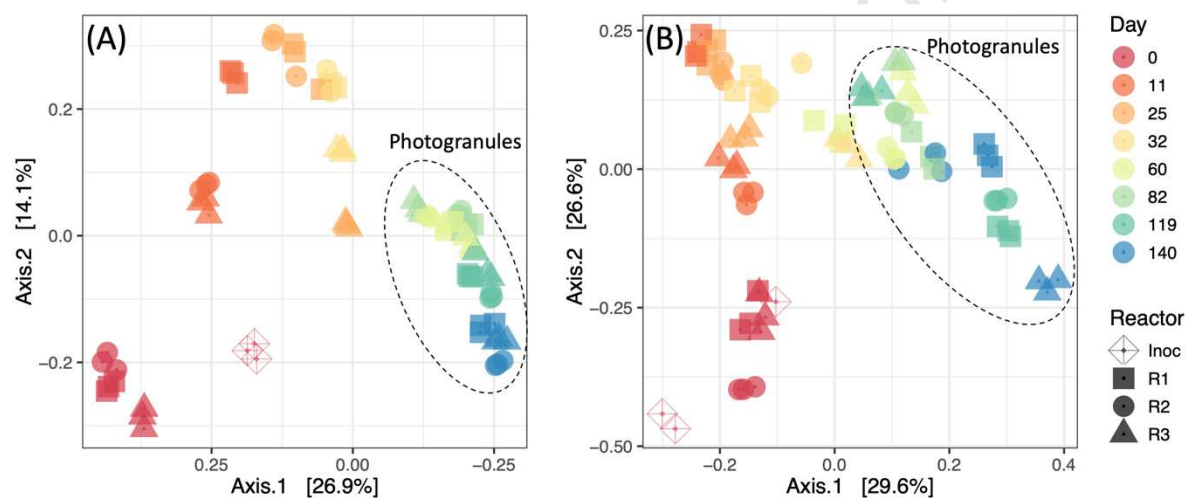
304   seed environment.

305

306   *Figure 4. Principal coordinates analysis (PCoA) was performed on the 16S (A) and 18S (B) gene sequences to explore the*
307   *similarities in between the set of triplicate measurements of each sampling day. This analysis demonstrates the overlap of*
308   *triplicate measurements and the trajectory of the microbial community to photogranules.*

309   **3.3.1.Prokaryotic community (16S)**

310   For the clustering analysis 61 OTUs were included related to functional groups in correspondence with

311   the MIDAS database (McIlroy et al., 2017) and Milferstedt et al. (2017b) (**table A4**). In addition, any

312   of the top 20 OTUs that were not assigned a functional group were also included giving a final total of

313   54. The functional groups included: phototrophs (19 taxa), biofilm former (3 taxa), filamentous

314   organism (13 taxa), nitrifiers (2 taxa), denitrifiers (6 taxa), polyphosphate accumulating organisms

315   (PAOs, 9 taxa) and methanotrophs (6 taxa). The analysis revealed four distinct bacterial communities

316   in the time series. Initially, the prokaryotic photosynthetic community was characterized by an

317   abundance of *Rhodobacter* (OTU_16), *Oscillatoria PCC-6304* (OTU_103), *Pseudanabaena PCC-*

318 *7429* (OTU_385), *Tychonema CCAP_1459-11B* (OTU_401), *Cyanobium PCC-6307* (OTU_819),

319 *Planktothricoides SR001* (OTU_1279) and *Phormidium ETS-05* (OTU_1374). This diverse

320 community of cyanobacteria decreased through time and was replaced in all reactors by a simplified

321 cyanobacterial community dominated by *Limnothrix* (OTU_4) (10%) and *Cephalothrix SAG 75.79*

322 (OTU_5) (11%). Other cyanobacterial OTUs such as *Leptolyngbya ANT-L52.2* (OTU_291),

323 *Leptolyngbya PCC-6306* (OTU_2) and *Alkalinema CENA528* (OTU_15) showed no distinct pattern

324 over the course of the experiment and exhibit a similar abundance at the beginning and the end of the

325 experiment.

326 Concomitant to the increase of the simplified photosynthetic community, the non-photosynthetic

327 prokaryotic reference taxa for biofilm formation, *Zoogloea* (OTU_12), *Thauera* (OTU_24) and

328 *Meiothermus* (OTU_7) increased. In all treatments *Zoogloea* became the most abundant organism at

329 the end of the time series with 13-18% relative abundance. In contrast, *Meiothermus* showed its

330 highest abundance (18%) at day 32 at HRT 1.00 d and then decreased in all reactors.

331 The nitrifying bacterial community was composed of only a single identified OTU, *Nitrosomonas*

332 (OTU_68) within the *Nitrosomonadaceae* family, which saw a general increase over time from the

333 inoculum. Several heterotrophic nitrifiers and aerobic denitrifiers were present in considerable

334 abundance such as *Comamonas* (OTU_23), *Zoogloea* (OTU_12), *Pseudomonas* (OTU_385),

335 *Diaphorobacter* (OTU_10), *Thauera* (OTU_24) and *Pelomonas* (OTU_202).

336 The functional group of PAOs showed a general increase over time except for *Gemmatimonas*

337 (OTU_313), which initially increased at HRT 1.00 and 0.67 with a sudden decrease most likely due to

338 washout. The most prominent representatives that increased were *Pseudomonas* (OTU_3),

339 *Acinetobacter* (OTU_18) and the novel cyanobacterial lineage *Obscuribacterales* (OTU_80), a

340 putative PAO enriched in a photo-EBPR system (Oyserman et al., 2017).

341 **3.3.2. Eukaryotic community (18S)**

342 In the majority of the sampling points, known photosynthetic organisms represented over 90% of the

343 eukaryotic community based on relative abundance. Initially, the photosynthetic fraction of the

16

344 eukaryotes was dominated by only three green algae *Chlorella sorokiniana* (OTU_1) (13%),

345 *Chlorococcum vacuolatum* (OTU_4) (32%) and *Desmodesmus sp. HSJ717* (OTU_43) (20%). Both

346 *Chlorella sorokiniana* (OTU_1) and *Chlorococcum vacuolatum* (OTU_4) were present in the initial

347 inoculum, but showed divergent patterns through time. In all reactors, *Chlorella sorokiniana* (OTU_1)

348 showed a steep increase until day 25, whereas, *Chlorococcum vacuolatum* (OTU_4) decreased in

349 relative abundance. Despite these divergent early trajectories, both populations eventually rebounded

350 and returned to similar relative abundances as in the beginning. In contrast, *Desmodesmus sp. HSJ717*

351 (OTU_43) generally showed a decrease in all reactors. In the final photosynthetic eukaryotic

352 community, a more diverse assemblage was found. Next to *Chlorella sorokiniana* (OTU_1) (23-29%)

353 and *Chlorococcum vacuolatum* (OTU_4) (8-19%), the community was enriched with *Scenedesmaceae*

354 *sp. A2_2* (OTU_78) (2-9%), *Chlamydomonadaceae sp. KMMCC_FC-97* (OTU_20) (5-7%) and

355 *Chlamydomonadales* (OTU_3) (14-16%).

356 The non-photosynthetic eukaryotic community was characterized by predatory eukaryotic organisms

357 such as rotifers, ciliates, amoeba and fungi. Amongst the predatory eukaryotic community, we

358 detected *Echinamoeba exundans* (OTU_119), *Spirotrichea* (OTU_29), *Bilateria* (OTU_69),

359 *Vermamoeba* (OTU_56), *Ascomycota* (OTU_168) and *Basidiomycota* (OTU_30). These taxa were

360 present in all sample points at very low levels except on day 140, when a sudden increase was

361 observed in all three reactors.

362 **3.4. Correlation network of microbial community, biomass characteristics and reactor function**

363 A correlation network using Pearson correlation coefficient (PCC) was carried out to assess the

364 relation between operational conditions, functional parameters and microbial community. In **figure 5**

365 the correlation network for all taxa, both prokaryotic and eukaryotic, show a positive correlation with

366 biomass characteristics (EPS, CNP content, SVI) and reactor performance (SE, nutrient removal). The

367 most connected nodes in the network are attributed to motile filamentous cyanobacteria, colony

368 forming photosynthetic eukaryotes, biofilm producing denitrifiers and organism involved in the

369 removal and conversion of nitrogen. SE, SVI and EPS content are strongly correlated to the

370 cyanobacteria *Limnothrix* (OTU_4) and *Cephalothrix SAG_75.79* (OTU_5) while EPS is correlated

371   with *Zoogloea* (OTU_12), *Thauera* (OTU_24), *Limnothrix* (OTU_4) and *Cephalothrix SAG_75.79*

372   (OTU_5). The node for EPS-PS is isolated from the rest of the network and is mostly correlated with

373   eukaryote *Desmodesmus* sp. *HSJ717* (OTU_43). From the network analysis it was shown that the total

374   nitrogen removal rate is mainly attributed to the phototrophic eukaryotes *Chlamydomonadaceae sp.*

375   *KMMCC_FC-97* (OTU_20) and *Chlamydomonadales* (OTU_3), and the non-phototrophic prokaryote

376   *Thauera* (OTU_24). Partial nitrification is largely correlated with *Comamonas* (OTU_23),

377   *Alicycliphilus* (OTU_9), *Pseudomonas* (OTU_3), *Nitrosomonas* (OTU_68) and *Diaphorobacter*

378   (OTU_10), while nitrification is correlated with *Diaphorobacter* (OTU_10) and an OTU from the

379   family *A4b* (OTU_137). In this network one taxa from the order of *Obscuribacterales* (OTU_80) is

380   present and is the only node connected to P removal. A significant correlation of three taxa from the

381   family *Microscillaceae* (OTU_76), *mle_1-27* (OTU_25) and the genus *Pelomonas* (OTU_202) with

382   phosphorus content of the biomass is observed. These organisms belong to the family of

383   *Comamonadaceae* that is often observed in wastewater treatment systems and show many putative

384   PAOs. Interestingly, *Leptolyngbya PCC-6306* (OTU_2) and other OTUs that were abundant

385   throughout such as *Acidovorax* (OTU_149), *Chlorella sorokiniana* (OTU_1) and *Chlorococcum*

386   *vacuolatum* (OTU_4) did not correlate with function, likely because they did not vary in relative

387   abundance through time as they were in high abundance in the inoculant and maintained this status as

388   abundant organisms.

389
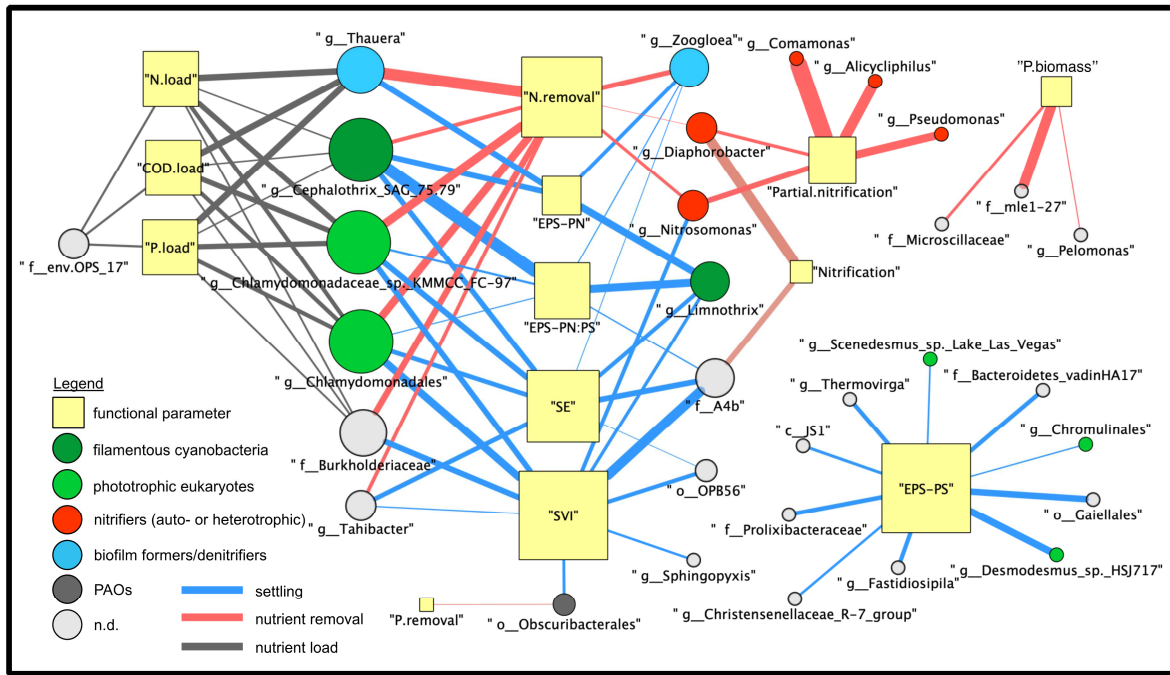
Figure 5. Network analysis of 16S/18S metagenomics and functional data on biomass characteristics and reactor function.
The functional network consists of taxa that strongly positively correlate with the attributed function. Functions of taxa and
kind of interaction is colour coded. The size of the nodes represents the connectivity of the taxa or reactor function. Edge
colour indicates the kind of relation and the thickness the correlation between two nodes.

4. Discussion

4.1. Photogranule formation

One of the most fundamental selection criteria for biomass in bioreactors is sedimentation. Effective settling and retention within the system is generally achieved through the formation of aggregates such as floc and granules. Organisms that do not participate in granule formation do not settle and therefore are washed out of the system. Here we show that applying lower HRT increases the rate at which granule formation is achieved. In all HRTs the EPS matrix makes a substantial part of the total photogranular biomass with no significant difference among them. The EPS obtained from photogranules at the end of the experiment showed an average EPS content of 239 ± 42 mg_{EPS} g_{VSS}^{-1} with a PN/PS ratio of about 6.6. This is lower than values found for aerobic granules (311 to 418 mg_{EPS} g_{VSS}^{-1}) however with a higher PN/PS ratio (3.4 to 6.2) (Adav and Lee, 2008). Our observation fall within the range of recent studies on photogranules that reported EPS values from 35.1 to 252.3 mg_{EPS} g_{VSS}^{-1} with an PN/PS ratio from 1.2 to 6.9 (Ansari, Abouhend and Park, 2019; Cai *et al.*, 2019, Kuo-Dahab *et al.*, 2018;).

The HRT had no consistent effect on the overall EPS-PN content, but generally lead to increasing PN/PS ratio at lower HRT. With increasing PN/PS ratio the SE increases while the SVI decreases (Figure 2A, **Figure A4**). These findings are in agreement with previous research on aerobic granules highlighted the importance of high PN/PS ratio for successful granulation (Adav et al., 2008; Pronk et al., 2017; Seviour et al., 2012). The high EPS-PN and low EPS-PS observed is attributed to increased hydrophobicity by decreasing the negative surface charge and excess Gibbs energy of the surface (Ding et al., 2015; Wilén et al., 2018). Activated sludge with floccular structure has usually a PN/PS ratio of around 0.9 that indicates low hydrophobicity (Adav and Lee, 2008). Polysaccharides contribute to the formation of cross-network structure with cells (Seviour et al., 2009). However, a higher polysaccharide compared to protein content is associated with floccular structures with loose morphology and slime properties (Flemming et al., 2007). The increase of the PN/PS from flocs (0.7) to photogranules (7.4) is in accordance with the change in surface properties of the biomass to photogranules (**Figure A3**).

20

4.2. Nutrient removal of a photogranular bioreactor

421

422 The maximum removal rate of 90 mg_N L^{-1} day^{-1} and 5.4 mg_P L^{-1} day^{-1} was three times higher than

423 similar photo-heterotrophic treatment systems (Liu et al., 2017; Van Den Hende et al., 2014, 2011;

424 Wang et al., 2015). The ammonical nitrogen removal, in particular, was improved through time due to

425 nitrification/denitrification which correlated with the change of the microbial community from flocs to

426 granules. Nitrification/denitrification are generally described as an additional nitrogen removal path in

427 the use of algal-bacterial communities (Arashiro et al., 2017; Oyserman et al., 2017; Rada-Ariza et al.,

428 2017; Van Der Steen et al., 2015). The consensus is that the assembly of microbes to flocs and

429 granules increases the stratification over the biomass and hence creates anoxic/anaerobic conditions in

430 the core, which would allow denitrifiers to convert nitrate into nitrogen gas (Adav et al., 2010).

431 An overall increase in volumetric nitrogen removal rate was observed with decreasing HRT from 2.00

432 to 0.33 days that was not proportional to the N assimilation in the biomass. This suggests that the

433 higher ammonium and COD loading at lower HRT had a positive effect on the nitrifying/denitrifying

434 community in the photogranules as shown by Princic *et al.*, (1998) for aerobic granules. The higher

435 nutrient loading could lead to a deeper penetration of nutrients in the granular structure and increased

436 denitrification (Alpkvist et al., 2006). The high abundance of *Zoogloea* and *Thauera*, both known

437 denitrifiers, could have influenced the N removal at HRT 0.67 and 0.33 days (**Figure A8**).

438 The main removal mechanism for P is via assimilation in biomass that matches with the biomass

439 productivity and P content (about 1%). Although the presence of several putative PAOs was detected

440 by 16S analysis, only *Obscuribacteriales* correlated with P removal, a finding in agreement with

441 Oyserman et al. (2017) which also saw the enrichment of this lineage under non-granular

442 photosynthetic feast-famine conditions. Carvalho et al. (2018) demonstrated as well the successful

443 implementation of photosynthetic cultures enriched in PAOs under feast famine conditions. In our

444 study, the enrichment of PAOs was not selected for directly. Incorporating the feast famine regime

445 that selects for PAO could increase the P removal of granular sludge while maintaining the benefits of

446 well-settling granular sludge.

447 **4.3. Community assembly of planktonic organisms to photogranules**

448 The two most abundant photosynthetic prokaryotic taxa, *Limnothrix* (OTU_4), *Cephalothrix*

449 *SAG_75.79* (OTU_5), are both motile filamentous cyanobacteria from the order of *Limnotrichales* and

450 *Nostocales*. These taxa are ubiquitous in nature but have not been reported previously to play an

451 important role in the formation of photogranules. They show great functional and morphological

452 similarities with the genus *Microcoleus*, a motile filamentous cyanobacteria previously found in

453 photogranules by Milferstedt et al. (2017b) and Stauch-White et al. (2017). In their research they

454 hypothesize that at least one motile filamentous cyanobacteria in high abundance is necessary to form

455 photogranules. Our results support these findings.

456 Our and previous reported findings confirm that these filamentous cyanobacteria have an important

457 role in the initiation of photogranulation. Interestingly, filamentous bacteria such as *Thiothrix* in

458 aerobic granules are generally unwanted since they lead to outgrowth and bulking sludge (de Kreuk,

459 2006). However, in the formation of anaerobic granular sludge the filamentous *Methanosaeta* is

460 thought to be crucial in granulation. This was proposed as the "Spaghetti theory" by Wiegant (1988).

461 In photogranulation a similar concept could be developed where filamentous organisms may become

462 entangled in microscopic knots which become the nucleus (a niche) for other organisms to attach and

463 form agglomerates that mature to granules.

464 With the assembly of photogranules, known biofilm producing prokaryotes such as *Zoogloea*

465 (OTU_12), *Thauera* (OTU_24) and *Meiothermus* (OTU_7) were enriched as granule formation

466 progressed. These organisms were previously reported as important for the assemblage of aerobic

467 granules by Weissbrodt *et al.*, (2013), and found to be a vital part of the microbial community in

468 aerobic granules incubated under photosynthetic conditions (Cai et al., 2019; Guo et al., 2018; Zhang

469 et al., 2018). As known biofilm and therefore EPS producers it is very likely that that they

470 substantially contribute to the granular matrix. However, it is not possible to state which organisms

471 contributed to what extend to the EPS matrix.

22

472   Interestingly, we saw that the washout conditions of decreasing HRT only dictated the time for

473   photogranule assembly, despite ending with similar microbial community structure (**Figure 4**). This

474   suggests that while HRT might not drive differences in final community structure of a granule, it does

475   increase the rate at which granule formation is achieved based on other functional parameters such as

476   SE, SVI and EPS. SRT could have a larger effect on the final algal-bacterial community as Bradley et

477   al., (2019) recently showed. Other operational choices such as settling time, feeding regime, nutrient

478   limitation, aeration or mechanical mixing would be interesting to test and evaluate the determining

479   effect on the community structure of photogranules.

480   **4.4. Network analysis of microbial community structure and reactor function – finding**

481   **biological drivers of physical and chemical properties in photogranules**

482   The network analysis showed that only a few organisms drive a wide array of functional parameters.

483   Microbes with the highest connectivity included the cyanobacteria *Limnothrix* (OTU_4), *Cephalothrix*

484   *SAG_75.79* (OTU_5) and the photosynthetic eukaryote *Chlamydomonadales* (OTU_3), suggesting

485   they may be key players in granule formation and community structure. Their strong correlation with

486   SVI, SE and PN/PS ratio indicates their structural importance in the photogranular makeup.

487   Additionally, they are related to nitrogen removal, which could be simply explained by their high

488   relative abundance. Interestingly, OTU 137 from the family of *A4b* showed a strong positive

489   correlation with SVI, SE and the PN/PS ratio of EPS as well. These taxa usually make up the core

490   microbial community of anaerobic digesters (Xia et al., 2016). Their presence could be an indicator for

491   dense granular structures that provide an anaerobic niche despite a highly aerated system. This is

492   especially seen in the relationship with SVI and *A4b,* which has the strongest correlation of all

493   organisms in the microbial community.

494   Conversely, the network analysis also showed that one parameter or function can be influenced by

495   many different organisms of the community in various degrees. Functions associated with the EPS

496   matrix are influenced by various organisms. *Zoogloea* (OTU_12), which was expected to strongly

497   correlate with EPS related functions only weakly correlates with EPS-PN. However, a strong

498   correlation with N content in the biomass and nitrogen removal rate was observed. *Thauera*

23

499 (OTU_24), another known EPS producer and prominent denitrifier, exhibits a much stronger

500 correlation to nitrogen removal than to EPS related functions (Adav et al., 2010). Although less

501 abundant it suggests that this taxon has a stronger influence on the functional parameters. The most

502 prominent being SVI, SE, EPS-PS and nitrogen removal. But also, other more conserved reactor

503 functions such as partial nitrification and nitrification are connected to many organisms of the

504 community especially of the genus *Nitrosomonas*, *Comamonas*, *Pseudomonas, Diaphorobacter*,

505 *Thauera* and *Pelomonas*.

506 As shown here, when starting with a suspended diverse microbial community and by applying the

507 right operational criteria such as phototrophic conditions, sedimentation and hydrodynamic, a

508 photogranular community can be formed. However, the question how to stir the microbial community

509 of the photogranule to improve desired traits such as nitrogen or phosphorus removal. Ideally

510 photogranule has excellent sedimentation, incorporates high nutrient removal rates and requires

511 minimum external input such as aeration. The photogranules obtained in this study show three times

512 higher (up to 90 mg_N L^{-1} day^{-1}) removal performance in comparison to other phototrophic systems, but

513 are still lower than other conventional treatment systems. For aerobic granular sludge operated at full

514 scale maximum volumetric removal rates are reported from 170 mg_N L^{-1} d^{-1} and 240 mg_P L^{-1} d^{-1} (Pronk

515 et al., 2015). This is 2 (for N) and 50 (for P) times higher than the volumetric removal rates obtained

516 here. To improve the nutrient removal rate of N and P the focus could be to improve the conditions for

517 higher nitrification rates and Enhanced Biological Phosphorus Removal (EBPR) by PAOs. This would

518 require additional operation strategies, which amongst others would include a sophisticated feeding

519 strategy, for example with providing feast/famine conditions of the primary nutrient (N, P, COD) as in

520 Oyserman et al. (2017). In this way another selection on nutrient limitation would be applied on the

521 microbial community that would promote organisms that produce storage compounds such as EPS,

522 lipids, polyhydroxyalkanoate, polyP. Due to the density of these polymers, it might be beneficial for

523 the overall treatment process by promoting settleability and nutrient removal, but might also be

524 interesting for later applications of the photogranular biomass. In addition, microalgae would fuel the

525 whole process by converting photonic energy into chemical energy, potentially excluding external

526 oxygen supply and reduce greenhouse gases such as CO_2 (Borowitzka and Moheimani, 2013).

527 **5. Conclusion**

528 • Low HRTs provide cyclic wash-out conditions in the bioreactors with a strong selective

529 pressure for well-settling biomass. Decreasing HRT improved settling, with a critical HRT

530 threshold of 1 day. Below this threshold, settling efficiency was above 95%, but above this

531 threshold separation efficiency stayed below 90%. Despite the differences between reactors in

532 HRT, after one month of operation all three reactors showed a similar microbial community

533 with floccular structure and good separation efficiencies.

534 • After three months of operation photogranules were obtained in all bioreactors. Decreased

535 HRT provides a 'shortcut' to produce well settling biomass (Figure 1), alters reactor

536 community structure more rapidly (Figure 4), and maintain high nutrient removal and reactor

537 function (Figure 2 & 3). Future research should be aimed to understand additional factors

538 related to granule formation such as SRT and nutrient feeding strategies, and parametrizing

539 them in combination with low HRT.

540 • The network analysis identified the key bacterial and eukaryotic taxa driving reactor functions.

541 The settling properties of the granules were most linked to motile filamentous cyanobacteria

542 (*Limnothrix*, *Cephalothrix SAG_75.79*), photosynthetic eukaryote *Chlamydomonadales* in

543 combination with EPS producers (*Zoogloea*, *Thauera*). The nutrient removal properties were

544 most linked to nitrifiers/denitrifiers (*Nitrosomonas*, *Comamonas*, *Thauera*, *Pseudomonas*,

545 *Diaphorobacter* and *Pelomonas*) and putative PAOs (*Obscuribacterales*).

546 • Compared to other photogranular system a different microbial assemblage was found but with

547 similar functional redundancy. Therefore, it might not be about specific strains but about

548 having (a) representative(s) from a function group with many potential strains. Further

549 research is needed to find out if the final community structure and function is decoupled and

550 depend mostly on the operation conditions rather than on the inoculum.

551

26

6. Acknowledgments

7. References

Abouhend, A.S., McNair, A., Kuo-Dahab, W.C., Watt, C., Butler, C.S., Milferstedt, K., Hamelin, J., Seo, J., Gikonyo, G.J., El-Moselhy, K.M., Park, C., 2018. The Oxygenic Photogranule Process for Aeration-Free Wastewater Treatment. Environ. Sci. Technol. 52, 3503–3511. https://doi.org/10.1021/acs.est.8b00403

Adav, S.S., Lee, D.J., 2008. Extraction of extracellular polymeric substances from aerobic granule with compact interior structure. J. Hazard. Mater. 154, 1120–1126. https://doi.org/10.1016/j.jhazmat.2007.11.058

Adav, S.S., Lee, D.J., Lai, J.Y., 2010. Microbial community of acetate utilizing denitrifiers in aerobic granules. Appl. Microbiol. Biotechnol. 85, 753–762. https://doi.org/10.1007/s00253-009-2263-6

Adav, S.S., Lee, D.J., Tay, J.H., 2008. Extracellular polymeric substances and structural stability of aerobic granule. Water Res. 42, 1644–1650. https://doi.org/10.1016/j.watres.2007.10.013

Alpkvist, E., Picioreanu, C., van Loosdrecht, M.C.M., Heyden, A., 2006. Three-dimensional biofilm model with individual cells and continuum EPS matrix. Biotechnol. Bioeng. 94, 961–979. https://doi.org/10.1002/bit.20917

Ansari, A.A., Abouhend, A.S., Park, C., 2019. Effects of seeding density on photogranulation and the start-up of the oxygenic photogranule process for aeration-free wastewater treatment. Algal Res. 40, 101495. https://doi.org/10.1016/j.algal.2019.101495

APHA/AWWA/WEF, 2012. Standard Methods for the Examination of Water and Wastewater. Stand. Methods 541. https://doi.org/ISBN 9780875532356

Arashiro, L.T., Rada-Ariza, A.M., Wang, M., Van Der Steen, P., Ergas, S.J., 2017. Modelling shortcut nitrogen removal from wastewater using an algal-bacterial consortium. Water Sci. Technol. 75, 782–792. https://doi.org/10.2166/wst.2016.561

Ardern, E., Lockett, W.T., 1914. Experiments on the oxidation of sewage without the aid of filters. J. Soc. Chem. Ind. 33, 523–539. https://doi.org/10.1002/jctb.5000331005

Borowitzka, M.A., Moheimani, N.R., 2013. Algae for Biofuels and Energy. https://doi.org/10.1007/978-94-007-5479-9

Bradley, I.M., Sevillano-Rivera, M.C., Pinto, A.J., Guest, J.S., 2019. Impact of solids residence time on community structure and nutrient dynamics of mixed phototrophic wastewater treatment systems. Water Res. 150, 271–282. https://doi.org/10.1016/j.watres.2018.11.065

Cai, W., Zhao, Z., Li, D., Lei, Z., Zhang, Z., Lee, D.J., 2019. Algae granulation for nutrients uptake and algae harvesting during wastewater treatment. Chemosphere 214, 55–59. https://doi.org/10.1016/j.chemosphere.2018.09.107

Cakir, F.Y., Stenstrom, M.K., 2005. Greenhouse gas production: A comparison between aerobic and anaerobic wastewater treatment technology. Water Res. 39, 4197–4203. https://doi.org/10.1016/j.watres.2005.07.042

594 Carvalho, V.C.F., Freitas, E.B., Silva, P.J., Fradinho, J.C., Reis, M.A.M., Oehmen, A., 2018. The impact of
595 operational strategies on the performance of a photo-EBPR system. Water Res. 129, 190–198.
596 https://doi.org/10.1016/j.watres.2017.11.010

597 de Kreuk, M.K., 2006. Aerobic Granular Sludge: Scaling up a new technology. TU Delft.

598 Ding, Z., Bourven, I., Guibaud, G., van Hullebusch, E.D., Panico, A., Pirozzi, F., Esposito, G., 2015. Role of
599 extracellular polymeric substances (EPS) production in bioaggregation: application to wastewater
600 treatment. Appl. Microbiol. Biotechnol. 99, 9883–9905. https://doi.org/10.1007/s00253-015-6964-8

601 DuBois, M., Gilles, K.A., Hamilton, J.K., Rebers, P.A., Smith, F., 1956. Colorimetric Method for Determination
602 of Sugars and Related Substances. Anal. Chem. 28, 350–356. https://doi.org/10.1021/ac60111a017

603 Fernandes, T. V., Shrestha, R., Sui, Y., Papini, G., Zeeman, G., Vet, L.E.M., Wijffels, R.H., Lamers, P., 2015.
604 Closing Domestic Nutrient Cycles Using Microalgae. Environ. Sci. Technol. 49, 12450–12456.
605 https://doi.org/10.1021/acs.est.5b02858

606 Fernandes, T. V., Suárez-Muñoz, M., Trebuch, L.M., Verbraak, P.J., Van de Waal, D.B., 2017. Toward an
607 Ecologically Optimized N:P Recovery from Wastewater by Microalgae. Front. Microbiol. 8, 1–6.
608 https://doi.org/10.3389/fmicb.2017.01742

609 Flemming, H.-C., Neu, T.R., Wozniak, D.J., 2007. The EPS Matrix: The "House of Biofilm Cells." J. Bacteriol.
610 189, 7945–7947. https://doi.org/10.1128/JB.00858-07

611 Guo, Y., Zhang, B., Bao, X., Cui, F., Shi, W., Zhang, R., Lens, P.N.L., Zhang, Z., 2018. The attachment
612 potential and N-acyl-homoserine lactone-based quorum sensing in aerobic granular sludge and algal-
613 bacterial granular sludge. Appl. Microbiol. Biotechnol. 102, 5343–5353. https://doi.org/10.1007/s00253-
614 018-9002-9

615 Henze, M., 2008. Biological wastewater treatment : principles, modelling and design LK -
616 https://wur.on.worldcat.org/oclc/236186544, TA - TT -. IWA Pub., London SE - 511 pages :
617 illustrations (some color) ; 29 cm.

618 Herlemann, D.P.R., Labrenz, M., Jürgens, K., Bertilsson, S., Waniek, J.J., Andersson, A.F., 2011. Transitions in
619 bacterial communities along the 2000 km salinity gradient of the Baltic Sea. ISME J. 5, 1571–1579.
620 https://doi.org/10.1038/ismej.2011.41

621 Hollander, M. de, 2018. nioo-knaw/hydra: 1.3.6. https://doi.org/10.5281/ZENODO.1434147

622 Huang, W., Li, B., Zhang, C., Zhang, Z., Lei, Z., Lu, B., Zhou, B., 2015. Effect of algae growth on aerobic
623 granulation and nutrients removal from synthetic wastewater by using sequencing batch reactors.
624 Bioresour. Technol. 179, 187–192. https://doi.org/10.1016/j.biortech.2014.12.024

625 Hugerth, L.W., Muller, E.E.L., Hu, Y.O.O., Lebrun, L.A.M., Roume, H., Lundin, D., Wilmes, P., Andersson,
626 A.F., 2014. Systematic design of 18S rRNA gene primers for determining eukaryotic diversity in microbial
627 consortia. PLoS One 9. https://doi.org/10.1371/journal.pone.0095567

628 Köster, J., Rahmann, S., 2012. Snakemake-a scalable bioinformatics workflow engine. Bioinformatics 28, 2520–
629   2522. https://doi.org/10.1093/bioinformatics/bts480

630 Lettinga, G., van Velsen, A.F.M., Hobma, S.W., de Zeeuw, W., Klapwijk, A., 1980. Use of the upflow sludge
631   blanket (USB) reactor concept for biological wastewater treatment, especially for anaerobic treatment.
632   Biotechnol. Bioeng. 22, 699–734. https://doi.org/10.1002/bit.260220402

633 Liu, L., Fan, H., Liu, Y., Liu, C., Huang, X., 2017. Development of algae-bacteria granular consortia in photo-
634   sequencing batch reactor. Bioresour. Technol. 232, 64–71. https://doi.org/10.1016/j.biortech.2017.02.025

635 Lowry, O.H., Rosebrough, N.J., Farr, A.L., Randall, R.J., 1951. Protein measurement with the Folin phenol
636   reagent. J. Biol. Chem. 193, 265–75. https://doi.org/10.1016/0304-3894(92)87011-4

637 Martin, M., 2013. Cutadapt removes adapter sequences from high-throughput sequencing reads. EMBnet.journal
638   17, 10–12. https://doi.org/10.14806/ej.17.1.200

639 McCarty, P.L., Bae, J., Kim, J., 2011. Domestic wastewater treatment as a net energy producer-can this be
640   achieved? Environ. Sci. Technol. 45, 7100–7106. https://doi.org/10.1021/es2014264

641 McIlroy, S.J., Kirkegaard, R.H., McIlroy, B., Nierychlo, M., Kristensen, J.M., Karst, S.M., Albertsen, M.,
642   Nielsen, P.H., 2017. MiDAS 2.0: An ecosystem-specific taxonomy and online database for the organisms
643   of wastewater treatment systems expanded for anaerobic digester groups. Database 2017, 1–9.
644   https://doi.org/10.1093/database/bax016

645 McIlroy, S.J., Saunders, A.M., Albertsen, M., Nierychlo, M., McIlroy, B., Hansen, A.A., Karst, S.M., Nielsen,
646   J.L., Nielsen, P.H., 2015. MiDAS: The field guide to the microbes of activated sludge. Database 2015.
647   https://doi.org/10.1093/database/bav062

648 McMurdie, P.J., Holmes, S., 2013. Phyloseq: An R Package for Reproducible Interactive Analysis and Graphics
649   of Microbiome Census Data. PLoS One 8. https://doi.org/10.1371/journal.pone.0061217

650 Meng, F., Liu, D., Huang, W., Lei, Z., Zhang, Z., 2019. Effect of salinity on granulation, performance and lipid
651   accumulation of algal-bacterial granular sludge. Bioresour. Technol. Reports 7, 100228.
652   https://doi.org/10.1016/j.biteb.2019.100228

653 Milferstedt, K., Hamelin, J., Park, C., Jung, J., Hwang, Y., Cho, S.-K., Jung, K.-W., Kim, D.-H., 2017a.
654   Biogranules applied in environmental engineering. Int. J. Hydrogen Energy 42, 27801–27811.
655   https://doi.org/10.1016/j.ijhydene.2017.07.176

656 Milferstedt, K., Kuo-Dahab, W.C., Butler, C.S., Hamelin, J., Abouhend, A.S., Stauch-White, K., McNair, A.,
657   Watt, C., Carbajal-González, B.I., Dolan, S., Park, C., 2017b. The importance of filamentous
658   cyanobacteria in the development of oxygenic photogranules. Sci. Rep. 7, 1–15.
659   https://doi.org/10.1038/s41598-017-16614-9

660 Morton, J.T., Toran, L., Edlund, A., Metcalf, J.L., Lauber, C., Knight, R., 2017. Uncovering the Horseshoe
661   Effect in Microbial Analyses. mSystems 2, 1–8. https://doi.org/10.1128/mSystems.00166-16

662   Oyserman, B.O., Martirano, J.M., Wipperfurth, S., Owen, B.R., Noguera, D.R., McMahon, K.D., 2017.

663   Community Assembly and Ecology of Activated Sludge under Photosynthetic Feast-Famine Conditions.

664   Environ. Sci. Technol. 51, 3165–3175. https://doi.org/10.1021/acs.est.6b03976

665   Oyserman, B.O., Noguera, D.R., Del Rio, T.G., Tringe, S.G., McMahon, K.D., 2016. Metatranscriptomic

666   insights on gene expression and regulatory controls in Candidatus Accumulibacter phosphatis. ISME J. 10,

667   810–822. https://doi.org/10.1038/ismej.2015.155

668   Paulson, J.N., Pop, M., Bravo, H.C., 2013. metagenomeSeq: Statistical analysis for sparse high-throughput

669   sequncing. http://www.cbcb.umd.edu/software/metagenomeSeq.

670   Princic, Mahne, Megusar, Paul, Tiedje, 1998. Effects of pH and oxygen and ammonium concentrations on the

671   community structure of nitrifying bacteria from wastewater. Appl. Environ. Microbiol. 64, 3584–90.

672   Pronk, M., de Kreuk, M.K., de Bruin, B., Kamminga, P., Kleerebezem, R., van Loosdrecht, M.C.M., 2015. Full

673   scale performance of the aerobic granular sludge process for sewage treatment. Water Res. 84, 207–217.

674   https://doi.org/10.1016/j.watres.2015.07.011

675   Pronk, M., Neu, T.R., van Loosdrecht, M.C.M., Lin, Y.M., 2017. The acid soluble extracellular polymeric

676   substance of aerobic granular sludge dominated by Defluviicoccus sp. Water Res. 122, 148–158.

677   https://doi.org/10.1016/j.watres.2017.05.068

678   Rada-Ariza, María, A., Lopez-Vazquez, C.M., Van der Steen, N.P., Lens, P.N.L., 2017. Nitrification by

679   microalgal-bacterial consortia for ammonium removal in flat panel sequencing batch photo-bioreactors.

680   Bioresour. Technol. https://doi.org/10.1016/j.biortech.2017.08.019

681   Seviour, T., Pijuan, M., Nicholson, T., Keller, J., Yuan, Z., 2009. Gel-forming exopolysaccharides explain basic

682   differences between structures of aerobic sludge granules and floccular sludges. Water Res. 43, 4469–

683   4478. https://doi.org/10.1016/j.watres.2009.07.018

684   Seviour, T., Yuan, Z., van Loosdrecht, M.C.M., Lin, Y., 2012. Aerobic sludge granulation: A tale of two

685   polysaccharides? Water Res. 46, 4803–4813. https://doi.org/10.1016/j.watres.2012.06.018

686   Smith, V.H., Sturm, B.S.M., deNoyelles, F.J., Billings, S.A., 2010. The ecology of algal biodiesel production.

687   Trends Ecol. Evol. 25, 301–309. https://doi.org/10.1016/j.tree.2009.11.007

688   Stauch-White, K., Srinivasan, V.N., Camilla Kuo-Dahab, W., Park, C., Butler, C.S., 2017. The role of inorganic

689   nitrogen in successful formation of granular biofilms for wastewater treatment that support cyanobacteria

690   and bacteria. AMB Express 7. https://doi.org/10.1186/s13568-017-0444-8

691   Su, G., Morris, J.H., Demchak, B., Bader, G.D., 2014. Biological Network Exploration with Cytoscape 3. Curr.

692   Protoc. Bioinforma. 47, 8.13.1-8.13.24. https://doi.org/10.1002/0471250953.bi0813s47

693   Tiron, O., Bumbac, C., Manea, E., Stefanescu, M., Lazar, M.N., 2017. Overcoming Microalgae Harvesting

694   Barrier by Activated Algae Granules. Sci. Rep. 7, 1–11. https://doi.org/10.1038/s41598-017-05027-3

695   Tiron, O., Bumbac, C., Patroescu, I. V., Badescu, V.R., Postolache, C., 2015. Granular activated algae for

696   wastewater treatment. Water Sci. Technol. 71, 832–839. https://doi.org/10.2166/wst.2015.010

697 Van Den Hende, S., Carré, E., Cocaud, E., Beelen, V., Boon, N., Vervaeren, H., 2014. Treatment of industrial
698   wastewaters by microalgal bacterial flocs in sequencing batch reactors. Bioresour. Technol. 161, 245–254.
699   https://doi.org/10.1016/j.biortech.2014.03.057

700 Van Den Hende, S., Vervaeren, H., Saveyn, H., Maes, G., Boon, N., 2011. Microalgal bacterial floc properties
701   are improved by a balanced inorganic/organic carbon ratio. Biotechnol. Bioeng. 108, 549–558.
702   https://doi.org/10.1002/bit.22985

703 Van Der Steen, P., Rahsilawati, K., Rada-Ariza, A.M., Lopez-Vazquez, C.M., Lens, P.N.L., 2015. A new photo-
704   activated sludge system for nitrification by an algal-bacterial consortium in a photo-bioreactor with
705   biomass recycle. Water Sci. Technol. 72, 443–450. https://doi.org/10.2166/wst.2015.205

706 Wang, M., Yang, H., Ergas, S.J., van der Steen, P., 2015. A novel shortcut nitrogen removal process using an
707   algal-bacterial consortium in a photo-sequencing batch reactor (PSBR). Water Res. 87, 38–48.
708   https://doi.org/10.1016/j.watres.2015.09.016

709 Weissbrodt, D.G., Neu, T.R., Kuhlicke, U., Rappaz, Y., Holliger, C., 2013. Assessment of bacterial and
710   structural dynamics in aerobic granular biofilms. Front. Microbiol. 4, 1–18.
711   https://doi.org/10.3389/fmicb.2013.00175

712 Wiegant, W.M., 1988. The "spaghetti theory" on anaerobic sludge formation, or the inevitability of granulation.
713   Granul. Anaerob. Sludge Microbiol. Technol. 146–152.

714 Wilén, B.-M., Liébana, R., Persson, F., Modin, O., Hermansson, M., 2018. The mechanisms of granulation of
715   activated sludge in wastewater treatment, its optimization, and impact on effluent quality. Appl. Microbiol.
716   Biotechnol. 102, 5005–5020. https://doi.org/10.1007/s00253-018-8990-9

717 Xia, Y., Wang, Yubo, Wang, Yi, Chin, F.Y.L., Zhang, T., 2016. Cellular adhesiveness and cellulolytic capacity
718   in Anaerolineae revealed by omics-based genome interpretation. Biotechnol. Biofuels 9, 1–13.
719   https://doi.org/10.1186/s13068-016-0524-z

720 Zhang, B., Lens, P.N.L., Shi, W., Zhang, R., Zhang, Z., Guo, Y., Bao, X., Cui, F., 2018. Enhancement of aerobic
721   granulation and nutrient removal by an algal–bacterial consortium in a lab-scale photobioreactor. Chem.
722   Eng. J. 334, 2373–2382. https://doi.org/10.1016/j.cej.2017.11.151

723

Highlights

- Lower HRT provides a 'shortcut' to well settling biomass and photogranules
- Motile filamentous cyanobacteria and EPS producer are important in photogranulation
- Correlation network analysis revealed key players in photogranulation
- Lower HRT increases overall volumetric removal rates
- Nitrification/denitrification is an important removal pathway in photogranules

Declaration of interests

☒ The authors declare that they have no known competing financial interests or personal relationships that could have appeared to influence the work reported in this paper.

☐The authors declare the following financial interests/personal relationships which may be considered as potential competing interests: